Article

Stability of the Steady-State Displacement of a Liquid Plug Driven by a Constant Pressure Difference along a Prewetted Capillary Tube

Sebastia#n Ubal, Diego M. Campana, María D. Giavedoni, and Fernando A. Saita

More About This Article

Additional resources and features associated with this article are available within the HTML version:

- Supporting Information
- Access to high resolution figures
- Links to articles and content related to this article
- Copyright permission to reproduce figures and/or text from this article

View the Full Text HTML

ACS Publications
High quality. High impact.

Stability of the Steady-State Displacement of a Liquid Plug Driven by a Constant Pressure Difference along a Prewetted Capillary Tube

Sebastián Ubal,[†,‡] **Diego M. Campana,**[†,‡] **María D. Giavedoni,**[*,†] **and Fernando A. Saita**[†]

INTEC (CONICET−Universidad Nacional del Litoral), Güemes 3450, 3000 Santa Fe, Argentina, and Facultad de Ingeniería, Universidad Nacional de Entre Ríos, Ruta Provincial 11, km 10, 3101 Oro Verde, Entre Ríos, Argentina

In this work we study the stability of a liquid plug driven along a capillary tube by a constant pressure difference. The methodology is based on the analysis of the values of the steady-state film thickness as a function of the plug length and the Capillary number, when the pressure drop and the Laplace number are fixed; thus, we extend our previous work where the plug was forced to move at a constant speed [Campana; et al. Stability of the steady-state motion of a liquid plug in a capillary tube. *Ind. Eng. Chem. Res.* **2007,** *46,* 1803]. The stability charts, built for selected values of the Laplace number and a wide range of the dimensionless parameters, show the existence of a small stable region whose size increases as the Laplace number is augmented.

1. Introduction

Liquid plugs are commonly encountered in a large number of technological applications such as oil recovery and microchannel reactors; also, they may form in the respiratory tree either naturally from an instability of the liquid film lining the walls of the smallest conduits during the expiration process in certain pathological conditions or from the instillation of a liquid for therapeutic purposes.

A prototype of this problem is the motion of a certain volume of liquid inside a capillary tube coated by a film of the same fluid. When the propagation is steady, the thickness of this film (the precursor film) must be equal to the thickness of the film left by the bubble traveling behind the plug (the deposited or trailing film). This steady motion might be the result of drawing out the front bubble with constant velocity or, more commonly, of applying a constant pressure drop between the front and the rear gas phases.

When the liquid plug is large, the gas phases can be regarded as semiinfinite bubbles traveling alone, and the flow problem can be split into two smaller ones (one for the rear meniscus of the leading bubble and the other one for the front meniscus of the trailing bubble, which are located ahead and behind of the plug, respectively).

The steady motion of a semiinfinite bubble in a capillary tube or between two closely spaced parallel plates initially filled with a liquid has been extensively studied analytically, numerically, and experimentally since the pioneering works of Taylor[1] and Bretherton.[2] The effect of inertia forces[3−5] and, more recently, the role played by soluble or insoluble surface active agents[6−8] on the system have been the topics of some of those works.

When the distance between the tips of two consecutive bubbles is small, the propagation of the plug is affected by the interaction of the gas phases, and the velocity and pressure fields must be simultaneously computed in the whole domain. The works on this subject are considerably less numerous, and, mainly motivated by the transport of liquid plugs in the pulmonary airways, the group led by Professor Grotberg carried out most of them. These studies theoretically or numerically investigated the effects of propagation speed, surfactants, and gravity on the motion and splitting of a liquid plug.

Fujioka and Grotberg[9] presented a numerical study on the steady propagation of a liquid plug in a small gap formed between two parallel plates; their analysis includes the effect of inertia forces, the length of the plug, and the ratio between inertia and capillary forces. The numerical scheme employed to solve the governing equations and boundary conditions is based on the finite volume technique and does not allow the authors to obtain solutions for Capillary numbers larger than 0.4 and plug lengths smaller than half the gap of the channel.

The effect of a soluble surfactant was studied analytically by Water and Grotberg[10] and numerically by Fujioka and Grotberg.[11] The first analysis is based on matched asymptotic expansions and lubrication theory and is valid for very small Capillary numbers, when the distance between the menisci is of the order of one tube radius and there are traces of surfactant in the liquid. The numerical study mentioned in the second place, solves the Navier−Stokes and continuity equations and the mass balance of surfactant with their boundary conditions using the SIMPLER algorithm together with a boundary fitted coordinate transformation.

To account for the effect of gravity, Suresh and Grotberg[12] presented an asymptotic analysis for the motion of a liquid plug between two parallel plates that form an angle equal to α with the direction of gravity; their analysis is valid for small Capillary number, negligible Reynolds number, and arbitrary Bond number. They obtained expressions for the trailing and leading film thickness as a function of α and the other dimensionless parameters, and quantified the asymmetry in the volume of liquid that is above and below the center plane of the channel.

Also in connection with the effect of gravity, Zheng et al.[13] numerically analyzed the effect of this variable on the steady motion of a liquid plug between parallel plates in Stokes flow regime and when the Reynolds number is finite. They studied the effects of the propagation speed, plug length, and surfactant transport on the distribution of the plug volume above and below the center plane, an important issue associated to the splitting of a plug in an airway bifurcation. Previous to this numerical work they reported experiments on the subject.[14]

* To whom correspondence should be addressed. Tel.: +54 342 4559174. Fax: +54 342 4550944. E-mail: madelia@santafe-conicet.gov.ar.
† INTEC. (E-mails: subal@santafe-conicet.gov.ar (S.U.); dcampana@santafe-conicet.gov.ar (D.M.C.); fasaita@santafe-conicet.gov.ar (F.A.S.)).
‡ Universidad Nacional de Entre Ríos.

An important point of the work by Fujioka and Grotberg[9] concerns the stability of the steady states computed. In fact, the authors conjecture that the lack of convergence of the numerical algorithm employed within a certain range of the parameters might be due to the nonexistence of stable steady states; i.e., if the steady-state solution is perturbed, the distance between the menisci will either continuously increase or decrease until the collapse of the plug.

To elucidate that point, we have recently studied[15] the stability of a liquid plug or a train of bubbles in the particular case in which the leading gas phase is forced to move at a constant speed. We employed a numerical algorithm based on the Galerkin/finite element method combined with the parametrization of the free surface by means of spines for the spatial discretization of the governing equations and their boundary conditions and on a finite difference scheme to march in time. The steady-state dimensionless film thickness, which is the more relevant parameter of our analysis, was drawn as a function of the dimensionless plug length within a large range of Reynolds number and for a Capillary number equal to 0.5, that is, for a value at which Fujioka and Grotberg could not obtain solutions for short plugs in the plane case situation.

Depending on the Reynolds number, two types of curves result when the steady-state values of the film thickness are depicted versus the plug length for a fixed Ca. From 0 up to a certain Re, the film thickness increases with the plug length until it becomes practically constant, while, for larger Re, this variable first diminishes and then levels off as the distance between the gas phases becomes longer.

On the basis of the shapes of the curves, the stability of the steady-state solutions was inferred and the assumptions were then verified by means of a transient numerical analysis. We concluded that it suffices to solve the steady-state problem to determine whether a steady liquid plug moving at constant velocity is stable or not.

In the present work we show how that methodology can be applied to study the stability of a liquid plug which propagates in a capillary tube coated with a layer of the same liquid, when the constant driving pressure difference between the front and rear gas phases is perturbed. The paper is organized as follows. In the next section the mathematical formulation of the problem is described; the main features of the numerical technique employed are listed in section 3, and selected numerical results are presented and discussed in section 4. Finally, section 5 concludes the work.

2. Mathematical Formulation of the Problem

We investigate the stability of the steady-state propagation of a liquid plug of length l_P in a capillary tube of radius R which is coated with a film of the same liquid whose thickness is h_∞^F. The density (ρ) and viscosity (μ) of the liquid as well as the surface tension (σ) at the gas/liquid interfaces are constant; the gas is regarded as inviscid so that only the fluid dynamics at the liquid phase is considered. The liquid plug is driven by a constant pressure difference between the trailing and front gas phases, $\Delta p = p_{BT} - p_{BF}$, and the pressure at the front gas phase, p_{BF}, is taken as the reference pressure and it is set equal to zero. As the plug propagates inside the tube, a liquid film with thickness h_∞^T is left behind the passage of the liquid lens; this film is called the deposited or trailing film, and in steady-state operation it has the same thickness than the precursor film, i.e. $h_\infty^F = h_\infty^T = h_\infty$. In our model, the frame of reference moves at a constant speed, U, equal to the steady-state displacement velocity of the liquid plug. When the motion is unsteady, the
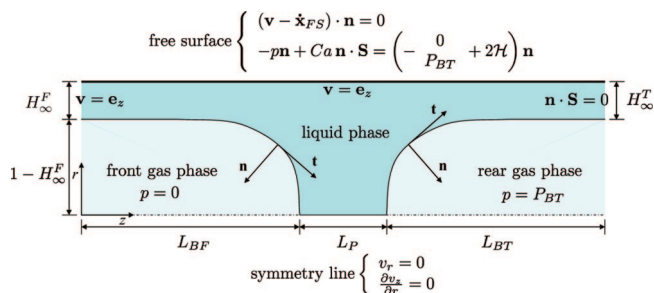

Figure 1. Schematic representation of the flow domain.

thickness of the trailing and leading films will generally be different, and both menisci will move with different speeds. The radius of the tube is small enough to consider negligible the action of gravity; therefore, the centerline of the tube is a symmetry line. Under these conditions, the conservation of mass and momentum in the liquid is described by the continuity and Navier–Stokes equations, which in dimensionless form reads

$$\nabla \cdot \mathbf{v} = 0 \qquad (1)$$

$$\lambda Ca\left(\frac{\partial \mathbf{v}}{\partial t} + \mathbf{v} \cdot \nabla \mathbf{v}\right) = -\frac{1}{Ca}\nabla p + \nabla \cdot \mathbf{S}, \quad \mathbf{S} = [\nabla \mathbf{v} + (\nabla \mathbf{v})^T] \qquad (2)$$

where $\mathbf{v}$ is scaled with U, p with σ/R, lengths with R, and time with R/U. The Laplace number is defined as $\lambda = \rho\sigma R/\mu^2$, and the Capillary number as $Ca = U\mu/\sigma$.

Boundary conditions imposed at the tube wall and at the centerline imply that the liquid adheres to the solid surface and that the centerline is a symmetry line (see Figure 1). Far away from the menisci, the liquid lining the wall of the tube is stagnant and viscous stresses vanish. The gas/liquid interfaces are material surfaces; therefore, the kinematic condition applies there

$$(\mathbf{v} - \dot{\mathbf{x}}_{FS}) \cdot \mathbf{n} = 0 \qquad (3)$$

where $\dot{x}_{FS}$ is the velocity of the free surface and $\mathbf{n}$ is the unit normal to the free surface, pointing into the gas phase. Because the temperature is constant and the system is free of surface active agents, the tangential component of the traction at each interface vanishes and the normal component is given by the following expression

$$-p\mathbf{n} + Ca\mathbf{n} \cdot \mathbf{S} = (-P_{Bi} + 2\mathscr{H}) \qquad (4)$$

In eq 4, $\mathscr{H}(t,\mathbf{x}_{FS})$ is the local mean curvature of the interface and P_{Bi} is the dimensionless pressure in the gas at the rear (P_{BT}) or the front (P_{BF}) of the plug.

When the propagation of the plug is steady, both the leading and trailing film thicknesses are equal and there is not relative motion between the menisci and the frame of reference. In our numerical algorithm, U (which is proportional to the Capillary number) is imposed, and $H_\infty = h_\infty/R$ and $\Delta P = P_{BT}$ are unknowns which are simultaneously calculated with the velocity and pressure fields, and with the interfacial shapes. When the motion is unsteady, $H_\infty^F \neq H_\infty^T$ and the tips of the bubbles might have a displacement velocity different from U (the velocity of the frame of reference); under these conditions, P_{BT} and H_∞^F are fixed and H_∞^T is calculated once the flow field is computed using the following expression,

$$Q = \int_{A_{out}} v_z \, dA = \pi H_\infty^T (2 - H_\infty^T) \qquad (5)$$

where Q is the flow rate evaluated at the annular outflow section (A_{out}).
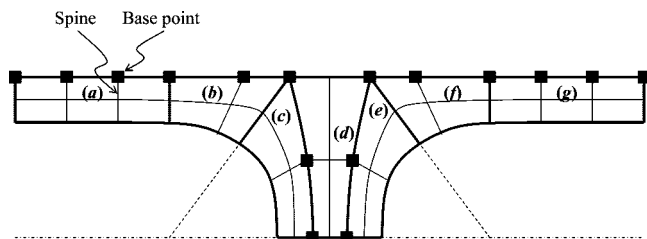
Figure 2. Sketch of the mesh showing the distribution of the spines and their base points. The regions of the mesh are also depicted.

In the next section, the numerical procedure employed to solve the governing eqs 1 and 2 with their boundary conditions is briefly explained.

3. Numerical Method

The system of governing equations and boundary conditions was solved with the same numerical technique employed in a previous work;[15] therefore, only its main features will be presented here. Nonetheless, we will underline the differences that exist between the actual and the previous implementation when computing the transient evolution of the system. The numerical scheme is based on the finite element method, and the velocity and pressure fields, as well as the shapes of the free surfaces, are simultaneously calculated. When the steady problem is solved for each selected value of Ca and λ, the driving pressure difference (ΔP) and the thickness of the leading and trailing films ($H_\infty = H_\infty^F = H_\infty^T$) are unknowns simultaneously obtained with the solution. On the other hand, when a transient case is considered, ΔP is fixed, H_∞^F is imposed and H_∞^T is evaluated as was previously done by using eq 5.

The spatial discretization of the problem is accomplished by a standard Galerkin/finite element formulation. The domain is tessellated into a structured mesh of Lagrange quadrilateral elements, which is conveniently divided into seven zones, labeled a–g in Figure 2.

In this work, the locations of both the inflow and outflow planes are kept constant during the computations; i.e., the distances L_{BF} and L_{BT} are not fixed. Those planes are located according to the expected behavior of the system; for instance, when the volume of the plug is presumed to indefinetely increase after the perturbation, they are placed far enough from the core region so that the evolution of the system can be followed satisfactorily during the computation. The axial length of the elements in the zone indicated as d in Figure 2 increases or diminishes as the distance L_P becomes longer or shorter, respectively, and that of the elements in a and g varies to fit changes in L_{BF} and L_{BT}, respectively. Also in order to reduce the distortion of the elements, the base points of the spines in regions c and e are now located on a curve and not on a straight line.

To select an appropriate finite element mesh, we looked for invariance of the solution with the size of the mesh and the distribution of the elements. As an example of the numerical tests carried out, we show in Figure 3 the steady-state free surface shapes and in Table 1 values of the film thickness and the driving pressure drop computed with three mesh refinements for $Ca = 0.1$, $\lambda = 1350$, and $L_P = 0.25$. In the table, DOF is the number of degrees of freedom and NOE is the total number of elements in each grid. Results reported in the figure show that the interfacial shapes computed with meshes 2 and 3 are almost identical; also, it is easy to see from the table that the relative difference between the values of H_∞ and ΔP computed
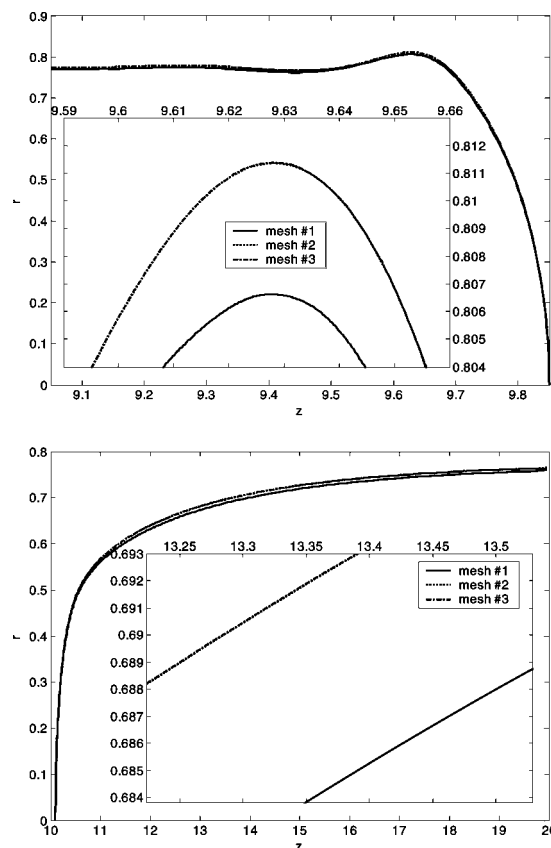
Figure 3. Free surface shapes computed for the three degrees of mesh refinement described in Table 1: Top, front gas phase; bottom, rear gas phase.

Table 1. Pressure Difference (ΔP) and Asymptotic Film Thickness (H_∞) Computed for Three Different Degrees of Mesh Refinement

	mesh 1	mesh 2	mesh 3
NOE	3984	10016	40064
DOF	39078	94357	368995
ΔP	3.05036	3.02702	3.02699
H_∞	0.229045	0.224520	0.224505

with those two meshes is smaller than 7×10^{-5} and 10^{-5}, respectively. Therefore, the meshes adopted to compute the solutions presented in this work are similar to mesh no. 2; in fact, they have between 10016 and 12608 elements depending on L_P, and they guarantee with a reasonable computational cost that the results are practically insensitive to a further refinement.

4. Results

As it was mentioned in the introduction, this work is the sequel of a previous one in which we analyzed the stability of a liquid plug which is forced to move at a constant speed inside a uniformly prewetted capillary tube; thus, the results of that study and those next discussed are structured in a similar way. That is, we first present solutions for the steady-state displacement; in particular, we illustrate the trend followed by the film thickness (H_∞) vs the length of the plug (L_P). From those curves, we inferred the stability of the system, and then, we carried out transient selected numerical computations to confirm our presumptions.

In this paper, we also depict the stability maps for selected values of the parameters and we discuss the location of the region where the steady-state solutions might be stable.

The properties of the system were chosen in order to encompass a large number of practical situations; in fact, the
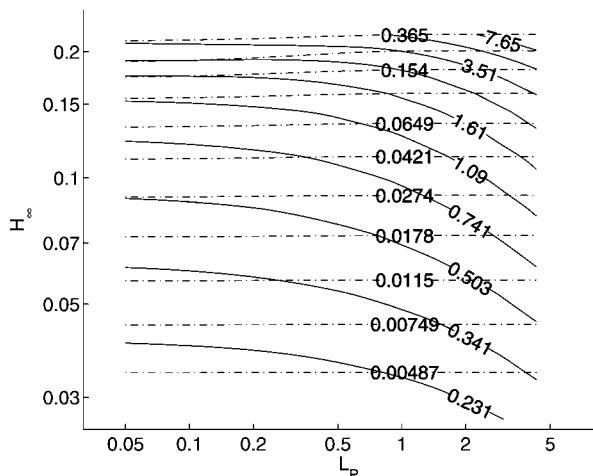
Figure 4. Steady-state film thickness as a function of plug length for $\lambda = 100$ and selected values of the Capillary number (dotted–dashed lines). Lines of constant ΔP are drawn in solid line.

Figure 5. Zoom of Figure 4, near the region where $(\partial H_\infty/\partial L_P)_{\Delta P} > 0$ (dash line).

speed of the plug was varied between 10^{-4} and 0.1 m/s, the liquid viscosity between 10^{-3} and 0.1 Pa s, the surface tension from 0.020 to 0.070 N/m, and the radius of the tube from 10^{-5} to 2×10^{-3} m. The liquid density was set equal to 1000 kg/m³, and the length of the plug was within the range of $0.05R \leq l_P \leq 4.3R$.

4.1. Steady-State Solutions. Consider a liquid plug of length L_P inside a capillary tube driven by a constant pressure drop ($\Delta P = P_{BT}$). For fixed liquid properties and a given tube radius, there is only one value of the displacement velocity for which the motion of the plug is steady; under these conditions, the films located behind and ahead of the plug have the same thickness ($H_\infty^T = H_\infty^F = H_\infty$), and the Laplace number $\lambda = Re/Ca = \rho\sigma R/\mu^2$ is a constant; i.e., any change in the velocity of the plug affects both the Capillary and the Reynolds numbers, keeping λ unchanged. If, during a short period of time, ΔP suffers a small perturbation, the system will depart from the steady state: the front and the rear gas phases will not necessarily travel at the same speed, and the length of the plug will change. Once the original pressure drop is reestablished, either one of the two following situations occurs: the system returns to the initial steady state, or it moves away from it. The former steady states will be regarded as stable while the latter ones will be considered unstable.

To study the stability of a plug driven by a constant pressure difference between the rear and front gas phases, we carried out computations for $\lambda = 100$, within a large range of Capillary numbers and for values of L_P between 0.05 and 4.3. In Figure 4, we depict the film thickness, H_∞, as a function of L_P; dotted–dashed lines correspond to a specific Capillary number and the solid ones to a given driving pressure drop.

From a quick examination of the curves along which ΔP is constant, one could conclude that they all have negative slope within the range of L_P here considered. However, a closer inspection (see Figure 5) indicates that there is a small region delimited by the dashed line, where $(\partial H_\infty/\partial L_P)_{\Delta P} > 0$. That is, for $\lambda = 100$ there is a range of Ca for which the film thickness corresponding to a given ΔP first increases and then decreases as L_P is augmented. This behavior is the basis of the following discussion regarding the stability of the steady motion of a plug driven by a constant pressure difference. It is worthy to note first that any two lines along which either ΔP or Ca is constant intercept each other. When one moves along a constant-ΔP curve in the direction of increasing L_P, Ca diminishes as a
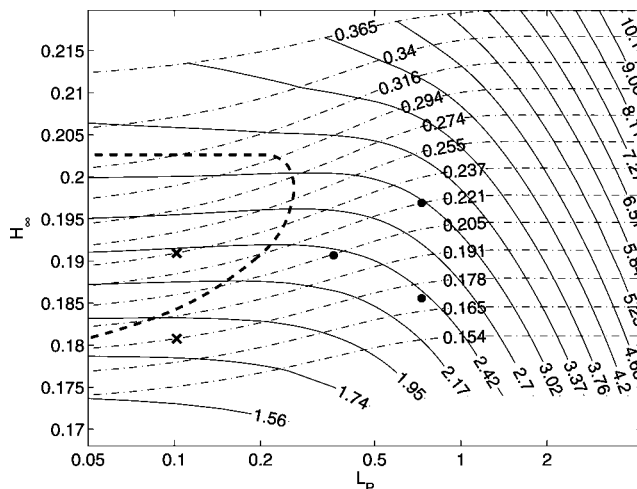
consequence of the smaller displacement velocity of the plug; a totally expected behavior because the same driving pressure difference is imposed across a larger amount of liquid. This smaller velocity is usually associated with a thinner steady film thickness.

Consider for instance a steadily advancing liquid plug corresponding to a point where $(\partial H_\infty/\partial L_P)_{\Delta P} > 0$ (i.e., inside the region delimited by a dashed line in Figure 5) and imagine that the driving pressure difference is suddenly increased by a small amount. As a result, the deposited film (H_∞^T) will become thicker while the thickness of the precursor film (H_∞^F) will remain the same. Therefore, the outflow rate will be larger than the inflow rate, and the distance between the front and the rear menisci will shorten; i.e., L_P will diminish. When, after a very short period of time, the original pressure drop is restored, H_∞^T will tend to be slightly smaller than H_∞^F, because the length of the plug is now somewhat smaller than the initial one. Consequently, the liquid accumulates between the gas phases until the initial state of the system is recovered; i.e., this state is stable. Also, if we imagine that ΔP is slightly reduced instead of increased, we will arrive to the same conclusion regarding the stability of the system.

With a similar reasoning, it is easy to see that any steady state located at a point where $(\partial H_\infty/\partial L_P)_{\Delta P} < 0$ is unstable. In fact, if ΔP is increased a little, the deposited film will become thicker while the precursor film will not change; thus, the outflow rate of liquid will be larger than the inflow rate and the distance between the menisci will diminish. When the driving pressure difference is reestablished, H_∞^T tends to be somewhat larger than H_∞^F producing a net flow of liquid out of the plug; therefore, the distance between the menisci will continuously diminish until another steady state is eventually achieved or the bubbles collapse. If ΔP is reduced by a small quantity, the deposited film becomes thinner and, thus, the gas phases move apart from one another. Once the original pressure drop is restored, H_∞^T tends to be somewhat thinner than H_∞^F, leading to the accumulation of more liquid between the menisci; therefore, L_P will continuously increase and the original configuration of the system will not be recovered.

From the above discussion, we argue that the points lying on a constant-ΔP curve for which $(\partial H_\infty/\partial L_P)_{\Delta P} < 0$ represent unstable steady states; those for which $(\partial H_\infty/\partial L_P)_{\Delta P} > 0$, correspond to stable steady states and, finally, the points at which $(\partial H_\infty/\partial L_P)_{\Delta P} = 0$ are neutrally stable. To verify those specula-
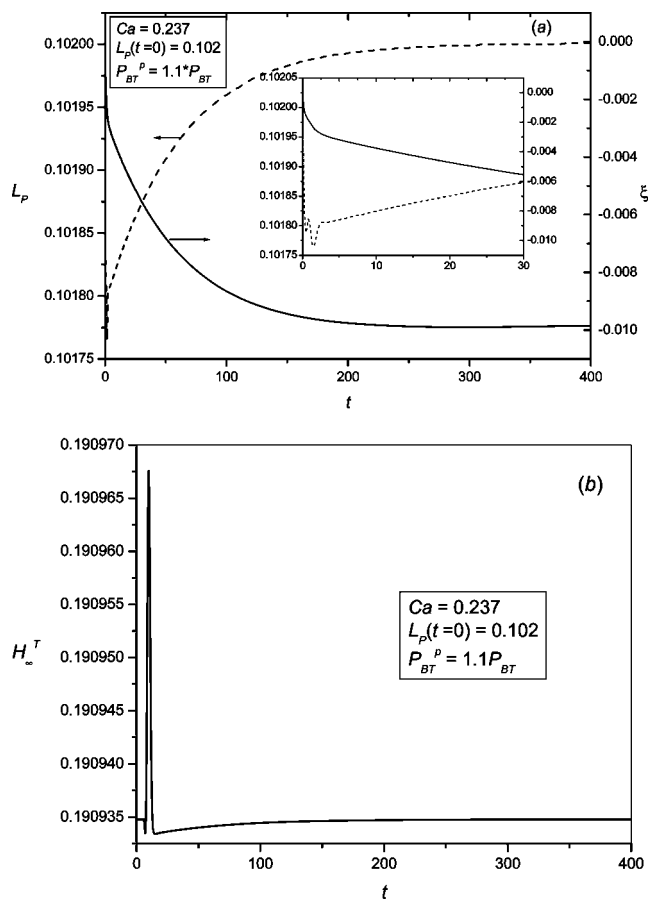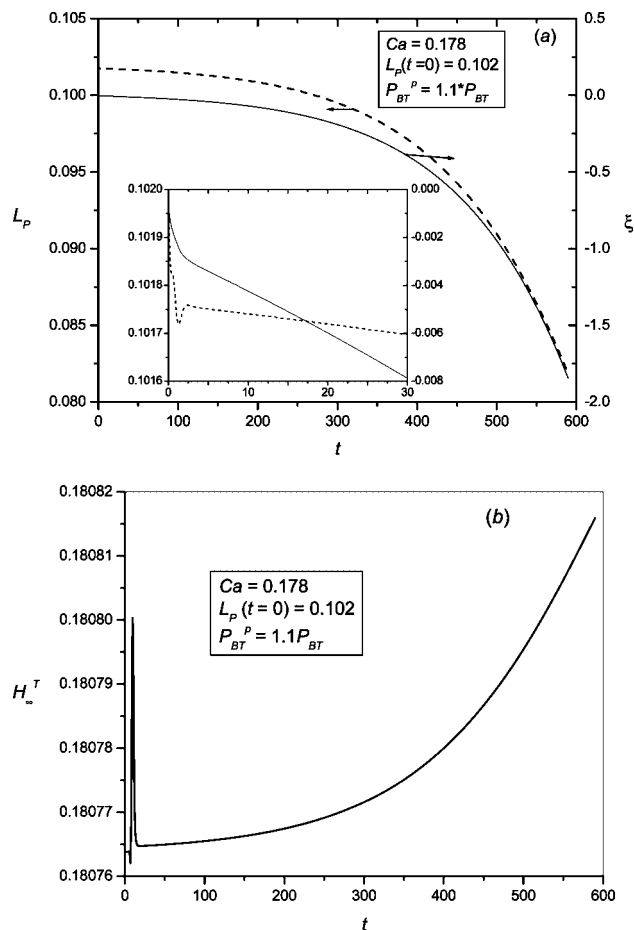
Figure 6. Time evolution of L_P and $\xi = z_P - z_P(t=0)$ (a) and of the deposited film thickness, H_∞^T, (b) after a 10% perturbation of the pressure at the back gas phase.

Figure 7. Time evolution of L_P and ξ (a) and of the deposited film thickness, H_∞^T, (b) after a 10% increase of the pressure at the rear gas phase.

tions, we perturbed a steady-state solution and numerically followed its evolution.

4.2. Transient Numerical Solutions. To assess the validity of the analysis presented in the above section, we designed numerical experiments that closely reproduce the situations described there. Starting from a steady-state solution, the pressure of the back gas phase (P_{BT}) is 10% either increased or decreased during the first 10 time steps ($0 \leq t \approx 0.02$), and then the original pressure drop is restored. The systems selected for the experiments are indicated with a cross in Figure 5.

Parts a and b of Figure 6 illustrate the transient evolution of a plug located inside the region presumed stable when a short positive pulse is applied to the back gas pressure (P_{BT}); the characteristic dimensionless numbers of this case are $Ca = 0.237$, $L_P = 0.102$, $P_{BT} = 2.3837$, and $\lambda = 100$. The moment just before the pressure pulse is applied, the liquid plug is at rest because we use a reference frame that moves with it; however, just at the instant a positive pressure pulse occurs, the plug starts to move toward the left since the reference frame is unchanged. The motion is given by $\xi(t)$ that measures the distance the central point of the plug has moved from its original location; i.e., $\xi = z_P - z_P(t = 0)$, where z_P is the plane amidst the tips at time t. It is easy to see that the abrupt increase in the pressure first affects the length of the plug that almost instantaneously reduces its length by $\cong 0.2\%$ and starts moving to the left. The nearly instantaneous reduction of L_P indicates that liquid is rapidly flowing outside the plug; actually, the pressure pulse produces a flow-rate pulse that travels downstream and is detected, as Figure 6b shows, at $t \approx 10.24$ when it reaches the boundary of the domain considered. Once the

pressure pulse has finished, the original value of ΔP is restored, but it is now applied to a shorter plug that accordingly moves faster than the steady-state case, leaving behind a film thinner than H_∞^F. Consequently, liquid begins to accumulate inside the plug and L_P increases toward its equilibrium value that is reached at $t \approx 270$.

The motion of the plug is in agreement with the process described above: its large initial velocity rapidly decreases once the pressure pulse has finished and the plug asymptotically comes to stop when $t \approx 270$.

If the applied pressure pulse is negative, the numerical solutions not presented here show that the plug also recovers the initial steady state, confirming our presumptions about its stability.

The other system selected in the analysis is defined by $Ca = 0.178$, $L_P = 0.102$, $P_{BT} = 1.83327$, and $\lambda = 100$, and results corresponding to the numerical evolution of a perturbation equal to 1.1 P_{BT} are depicted in Figure 7a,b.

Also in this case, L_P and ξ are the variables which first notice the perturbation; nevertheless, the evolution of these variables now show that the menisci continuously approach one another and that the displacement velocity of the plug (inferred from the curve of ξ vs t) increases monotonically until it eventually ruptures because the rear and front gas phases contact. Actually, with the mesh adopted for this particular case the evolution of the gas phases can only be predicted until the distance between the tips is nearly 0.08.

Similarly to the previous example, the perturbation is not detected immediately at the outflow plane; the deposited film thickness presents a small maximum at $t \approx 10$, and then this
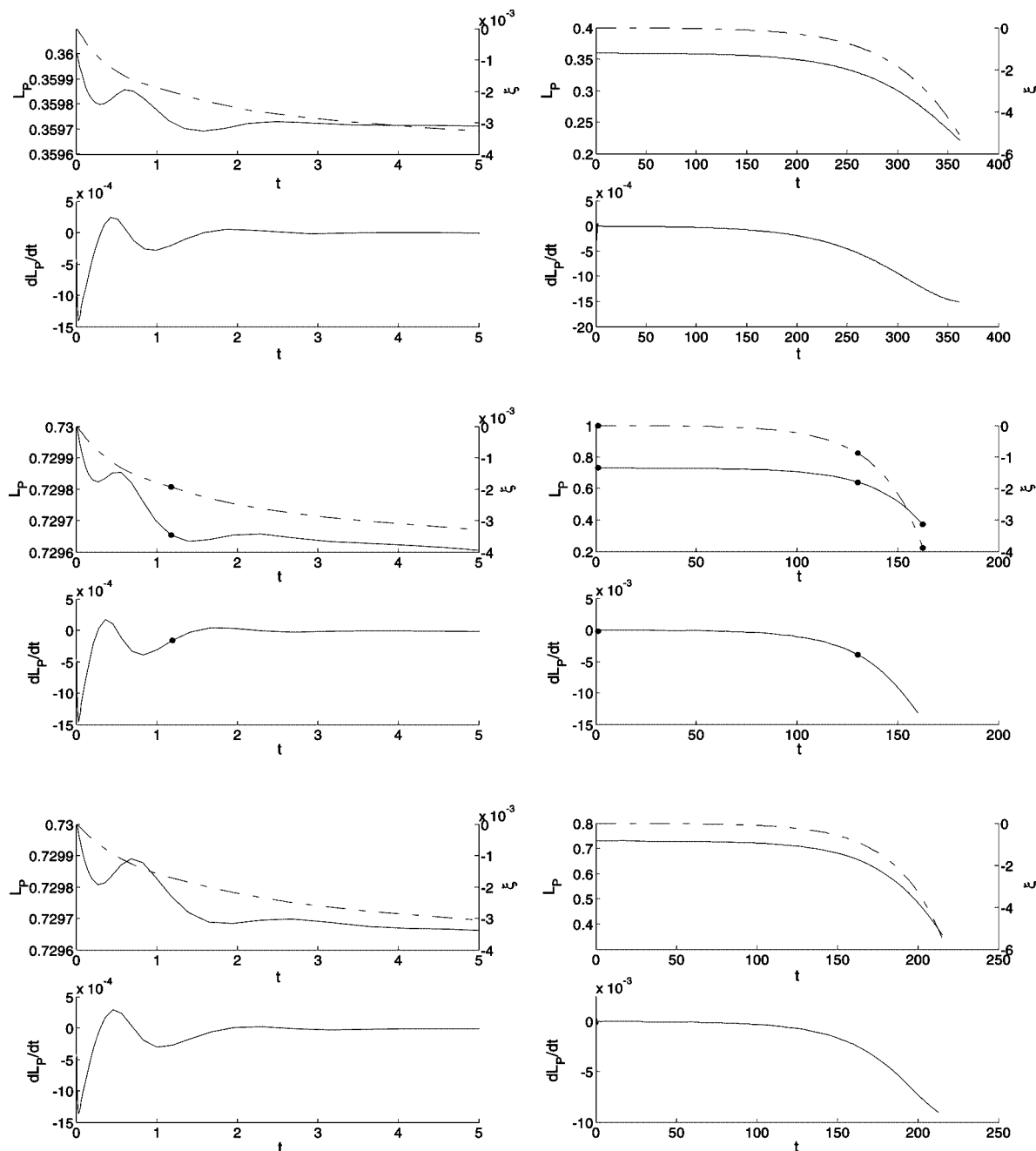
Figure 8. Time evolution of L_P, ξ ($-\cdot-$) and dL_P/dt. From top to bottom, $Ca = 0.2046$, $L_P = 0.36$; $Ca = 0.1710$, $L_P = 0.73$; and $Ca = 0.221$, $L_P = 0.73$, after a 10% increase of the pressure at the rear gas phase.

variable increases monotonically until the end of the computation inducing a continuous flow of liquid out of the plug.

If P_{BT} is 10% reduced instead of increased, the numerical solutions (not presented here) show the same results regarding the stability of the plug, but in this case the distance between the front and the rear interface increases after the perturbation. To determine the magnitude of this perturbation, we took into account that a 10% disturbance of the pressure produces approximately a 0.1% initial variation of L_P.

From the results of the previous numerical experiments we conclude that the analysis carried out in the previous section is useful to assess the stability of the steady displacement of a liquid plug driven by a constant pressure difference. Moreover, the transient evolution of the plug computed numerically is qualitatively very similar to that imagined from the steady-state solutions portrayed in Figure 5.

It might be interesting to analyze the influence of the slope of the constant$-\Delta P$ curve on the time required for the collapse. To this end, we studied the transient evolution of the various plugs identified with a dot in Figure 5, and the results obtained are depicted in Figure 8. We first consider the plugs characterized by $Ca = 0.2046$, $L_P = 0.36$ and $Ca = 0.171$, $L_P = 0.73$, respectively, which are located on the curve $\Delta P = 2.38$. When the driving pressure is 10% increased during a very short interval of time and is then restored, the distance between the menisci continuously diminishes, confirming that both steady states are unstable. The curves for the time derivative of L_P show that the velocity at which the gas phases approach each other rises as the initial plug length and $(\partial H/\partial L_P)_{\Delta P}$ become larger. In fact, for the plug mentioned in the first place, the speed at which the tips come closer is of order 10^{-3}, while, for the latter one, it is of order 10^{-2}.
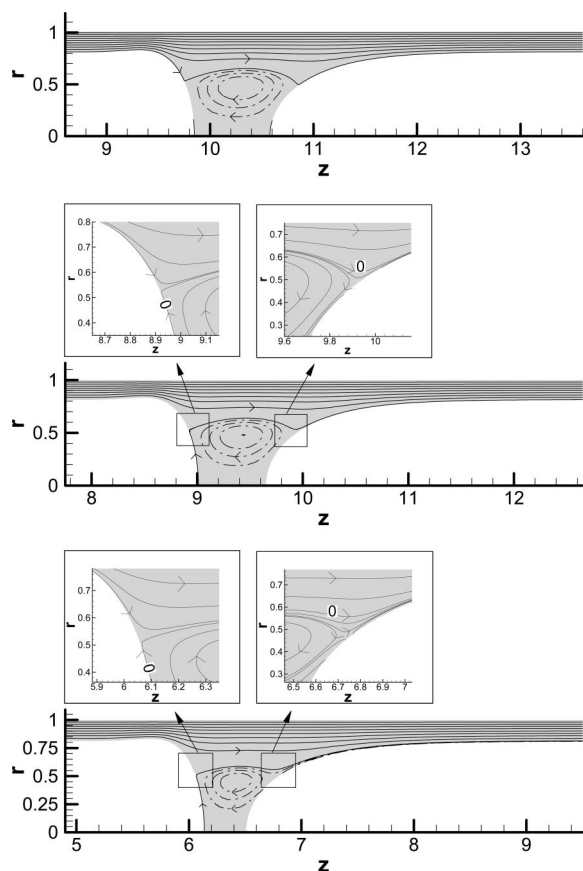
Figure 9. From top to bottom: instantaneous streamlines for $Ca = 0.1710$, $L_P = 0.73$, $\lambda = 100$, at $t = 1.18$, $t = 130.1$, and $t = 162.2$.

We examine now the plug whose length is also equal to 0.73 but is located on the curve $\Delta P = 2.99$ ($Ca = 0.221$). Although it is not easy to see from Figure 5, $(\partial H/\partial L_P)_{\Delta P=2.99}$ is slightly smaller than $(\partial H/\partial L_P)_{\Delta P=2.38}$. Results illustrated in Figure 8 point out that once the plug is perturbed, the menisci move toward each other with a slightly smaller velocity than when $Ca = 0.171$; for instance, the time elapsed when L_P reduces from 0.73 to 0.40 is 50 units of dimensionless time longer than in the previous case.

The temporal evolution of $\xi(t)$ illustrated in Figure 8 shows that, after the perturbation, the dimensionless speed of the plug is barely larger than 1 (i. e., the dimensionless velocity of the frame of reference); considering the characteristic scales employed for time and length, it is straightforward to see that the distance traveled by the plug before the simulation crashes is indeed quite large in the three cases (about $360R$ for $Ca = 0.2046$, $L_P = 0.36$; $160R$ for $Ca = 0.171$, $L_P = 0.73$; and $210R$ for $Ca = 0.221$, $L_P = 0.73$).

The above analysis suggests that the system moves away faster from an unstable steady state whenever the slope of the curve of H_∞ vs L_P is larger.

To complete the analysis of the transient evolution of the system, we calculated the stream function at selected instants of time in all the unstable cases discussed above. To make the interpretation of the resulting instantaneous streamlines simpler, we used here a reference frame that moves with the front tip of the plug. Since the chronological sequence of patterns are very similar in the four situations considered, we only discuss here the streamlines for $Ca = 0.1710$, $L_P = 0.73$, and $\lambda = 10^2$. These streamline patterns are portrayed in Figure 9 for the three instants of time marked with dots in Figure 8; they correspond to the beginning of the process, to an intermediate point, and to an

instant near the end of the computation, respectively. There are two sets of streamlines in Figure 9, each of them plotted at equally spaced levels; one set is associated with negative stream function values (solid lines) and the other one, which shows the flow in the core region, with positive stream function values (dashed−dotted lines).

The streamline pattern for $t = 1.180$ resembles that of the steady state in which four stagnation points are present: two at the tips and the other two on each interface. The similarities between both patterns are due to the very small speed at which the length of the plug is decreasing (see Figure 8) and to the fact that far away from the menisci the thickness of the precursor and deposited films and are almost equal.

Differences between the flow patterns for $t = 130.1$ and the steady state are easily detected in the second picture, agreeing with the larger dimensionless speed at which L_P diminishes (see Figure 8). In fact, there is a streamline —the one indicated with the letter O—that starts at the rear tip and moves along the centerline and the front interface, and finally it is directed toward the trailing film region. Details of the flow field for the regions enclosed in the rectangles are depicted in the insets. The more salient feature is the saddle point located near the region where the streamlines that detach from the rear interface are directed either downward or upward (see the inset at the right); another characteristic which can be observed in the inset placed at the left are the streamlines which begin at the front interface and go into the film region.

As the process continues and the distance between the menisci shortens, the saddle point moves away from the interface and the size of the recirculation diminishes along both the z- and the r-coordinates as it can be observed in the snapshot for $t = 162.2$. This is due to the relatively larger extension of the domain where the fluid is flowing from the rear interface toward the film region.

From the analysis of the evolution of the shapes of both interfaces, we can conclude that they remain almost the same during the whole process.

In the next section we present the stability maps for selected values of the Laplace number.

4.3. Stability Maps. To detect the influence of λ on the location of the parameter region where the steady-state displacement of a plug is stable, we carried out numerical computations for $\lambda = 10$, 10^3, and 10^4 within the range of Capillary numbers and plug lengths previously established. The computed values of H_∞ and ΔP for each set (L_P, Ca) were used to draw stability charts similar to those depicted in Figures 4 and 5.

From the analysis of the map corresponding to $\lambda = 10$, that is not depicted here, we conclude that all the curves corresponding to a fixed driving pressure drop have a negative slope, pointing out that for this particular value of the Laplace number the steady propagation of any plug is unstable for $0.0001 \le Ca \le 1$, and $0.05 \le L_P \le 4.3$.

Results reported in Figures 10a,b and 11a,b together with those depicted in Figures 4 and 5 show that as the Laplace number increases, i.e., as both inertia and surface tension forces turn relatively more important than viscous forces, the stable region extends over a larger range of Ca and L_P values. For each λ selected, the stable region always encompasses short plugs moving at relatively high velocities; moreover, according to our numerical solutions the estimated upper limit of this zone seems to be a line where H_∞ is nearly constant for a certain ΔP. This line represents marginally stable plugs, which move with a decreasing velocity as the length of the plug increases,
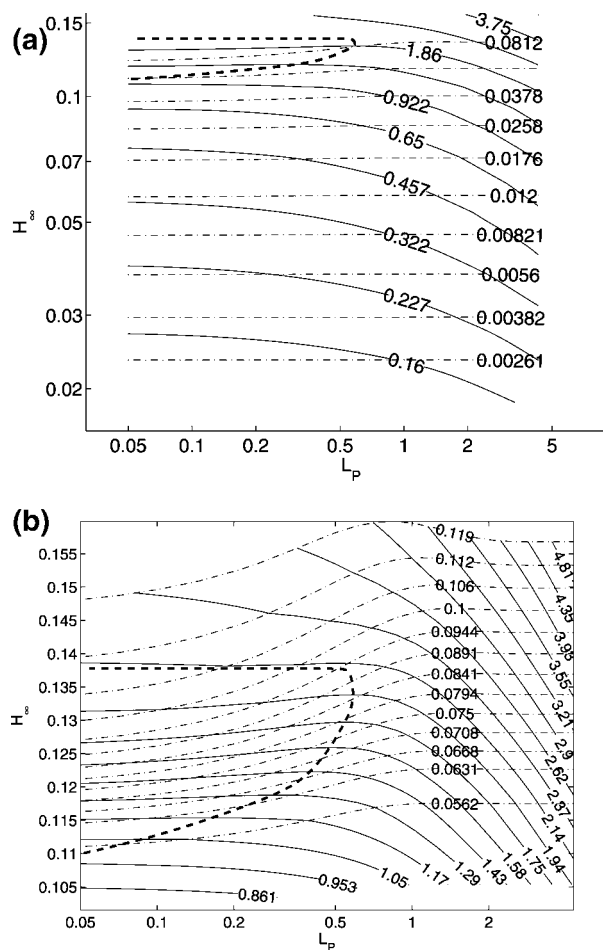
Figure 10. (a) Steady-state film thickness as a function of plug length for $\lambda = 10^3$ and selected values of the Capillary number (dotted−dashed lines). Lines of constant ΔP are drawn as solid lines. The region where $(\partial H/\partial L_P)$ > 0 is approximately delimited by a dashed line. (b) Enlarged view of the region delimited by a dashed line in a.

Figure 11. (a) Steady-state film thickness as a function of plug length for $\lambda = 10^4$ and selected values of the Capillary number (dotted−dashed lines). Lines of constant ΔP are drawn as solid lines. The region where $(\partial H/\partial L_P)$ > 0 is approximately delimited by a dashed line. (b) Enlarged view of the region delimited by a dashed line in a.
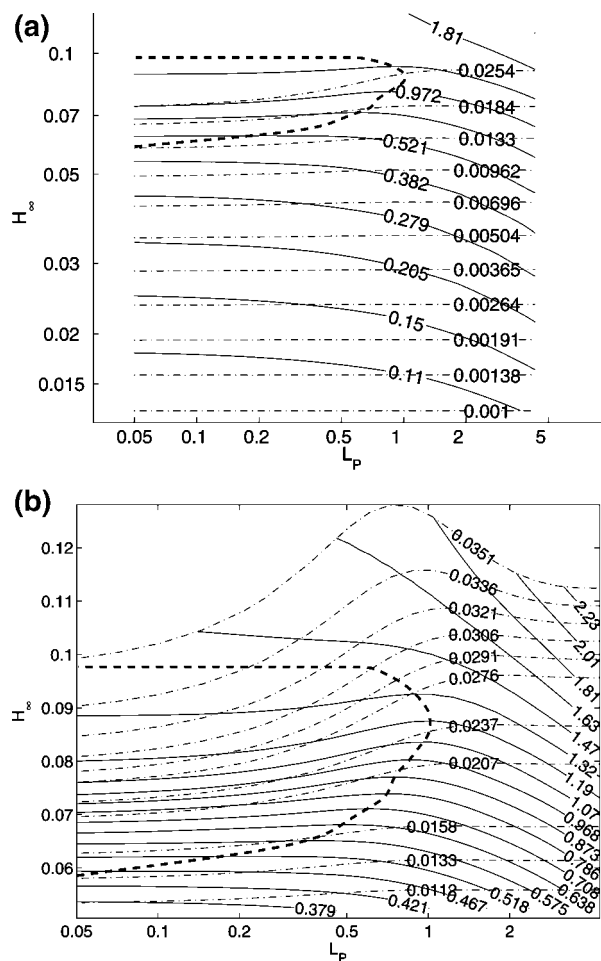
the thickness of the film coating the tube wall being nearly the same in all of them.

Another feature of the results illustrated in those figures is that the maximum length of a stable plug is approximately equal to the tube radius (for $\lambda = 10^4$); also when the distance between the front and rear gas phases is large enough so that they do not interact, the steady states are always unstable in the range of λ selected in this work.

5. Conclusion

In this paper we extended the methodology presented in a previous work[15] to study the stability of the steady displacement of a liquid plug forced to move at a constant speed to the more common situation in which the plug is driven by a constant pressure difference between the front and the back gas phases. To this end, the curves of the steady-state film thickness versus the length of the liquid plug for a fixed value of both the Capillary number and the driving pressure difference were built for selected values of the Laplace number. With similar arguments to those used previously, we related the slope of H_∞ versus L_P to the stability of the solutions, and we then confirmed our arguments perturbing the steady state and following its evolution numerically.

The results of this work together with those of our former paper[15] lead to the conclusion that it suffices to solve the steady-state problem to determine whether a steady-state plug is stable or not.

The stability maps built show that the region where the steady-state displacements are stable becomes larger as the Laplace number increases; moreover, this region encompasses liquid plugs with lengths as large as the tube radius when $\lambda = 10^4$; a particularly interesting result if one takes into account that for air−water and most air-aqueous solution systems, this parameter is approximately equal to 70000.

Literature Cited

(1) Taylor, G. I. Deposition of viscous fluid on the wall of a tube. *J. Fluid Mech.* **1961**, *10*, 161.

(2) Bretherton, F. P. The motion of long bubbles in tubes. *J. Fluid Mech.* **1961**, *10*, 166.

(3) Giavedoni, M. D.; Saita, F. A. The axisymmetric and plane cases of a gas phase steadily displacing a Newtonian liquid-A simultaneous solution of the governing equations. *Phys. Fluids* **1997**, *9*, 2420.

(4) Giavedoni, M. D.; Saita, F. A. The rear meniscus of a long bubble steadily displacing a Newtonian liquid in a capillary tube. *Phys. Fluids* **1999**, *11*, 786.

(5) Heil, M. Finite Reynolds number effect in the Bretherton problem. *Phys. Fluids* **2001**, *13*, 2517.

(6) Wassmuth, F.; Laidlaw, W. G.; Coombe, D. A. Calculation of interfacial flows and surfactant redistribution as a gas-liquid interface moves between two parallel plates. *Phys. Fluids A* **1993**, *5*, 1533.

(7) Ghadiali, S. N.; Gaver, D. P., III. The influence of non-equilibrium surfactant dynamics on the flow of a semi-infinite bubble in a rigid cylindrical capillary tube. *J. Fluid Mech.* **2003**, *478*, 165.

(8) Severino, M.; Giavedoni, M. D.; Saita, F. A. A gas phase displacing a liquid with soluble surfactants out of a small conduit: The plane case. *Phys. Fluids* **2003**, *15*, 2961.

(9) Fujioka, H.; Grotberg, J. B. Steady propagation of a liquid plug in a two-dimensional channel. *ASME J. Biomech. Eng.* **2004**, *126*, 527.

(10) Waters, S. L.; Grotberg, J. B. The propagation of a surfactant laden liquid plug in a capillary tube. *Phys. Fluids* **2002**, *14*, 471.

(11) Fujioka, H.; Grotberg, J. B. The steady propagation of a surfactant-laden liquid plug in a two-dimensional channel. *Phys. Fluids* **2005**, *17*, 082102.

(12) Suresh, V.; Grotberg, J. B. The effect of gravity on liquid plug propagation in a two-dimensional channel. *Phys. Fluids* **2005**, *17*, 031507.

(13) Zheng, Y.; Fujioka, H.; Grotberg, J. B. Effects of gravity, inertia, and surfactant on steady plug propagation in a two-dimensional channel. *Phys. Fluids* **2007**, *19*, 082107.

(14) Zheng, Y.; Fujioka, H.; Grotberg, J. C.; Grotberg, J. B. Effects of inertia and gravity on liquid plug splitting at a bifurcation. *ASME J. Biomech. Eng.* **2006**, *128*, 707.

(15) Campana, D. M.; Ubal, S.; Giavedoni, M. D.; Saita, F. A. Stability of the steady-state motion of a liquid plug in a capillary tube. *Ind. Eng. Chem. Res.* **2007**, *46*, 1803.